SASBE 2025 aims to encourage the international exchange of innovative ideas between researchers from academia and industry. In addition to knowledge dissemination, the conference offers a valuable platform for professional networking, particularly benefiting university professors, graduate students, and postdoctoral researchers.

Research Article/ Review Article/ Perspective Article (Remove where relevant)

Geospatial Assessment of Deglaciation and Climate Change Impacts in Chandra Valley, Western Himalaya (1989–2017)

Sadiq Ali Nabawi

PhD Student, Department of Studies in Earth Science, University of Mysore, India
Correspondence: sadiqnabawi20234@gmail.com

Copyright: Copyright: © 2025 by the authors.

SASBE is an open-access proceedings distributed under the terms of the Creative Commons Attribution 4.0 International License (CC BY 4.0).
View this license's legal deed at https://creativecommons.org/licenses/by/4.0/

Abstract

Glacier retreat in the Himalaya is a visible indicator of climate change with implications for water security, hazards, and ecosystems. We present a geospatial assessment of glacier change in the Chandra Valley, Western Himalaya (India) from 1989–2017 using multi-temporal Landsat 5 TM / Landsat 8 OLI imagery supported by ALOS PALSAR DEM. A hybrid workflow (supervised classification with visual interpretation and terrain constraints) delineated five elements—accumulation area (AA), ice-exposed ablation (IEA), debris-covered ablation (DCA), deglaciated valley (DV), and glacial lakes (GL)—which were compared across epochs and intervals.

Total glacier area declined from 726.36 km^2 (1989) to 614.45 km^2 (2017) (−111.91 km^2; ≈15%). Over the same period, AA decreased by 74.75 km^2, IEA by 23.58 km^2, and DCA by 13.59 km^2; DV expanded by 29%, and GL increased by 51%, indicating enhanced downwasting, forefield exposure, and lake growth. These results evidence accelerating cryospheric change with cascading impacts on downstream water resources, hydropower reliability, and community resilience.

By quantifying long-term, feature-resolved changes and interval contrasts, this study supports climate-adaptation planning and underscores the need for sustained monitoring and integrated policies for water management and disaster preparedness in debris-rich Himalayan catchments.

Keywords: Western Himalaya; Chandra Valley; Glacier Change; Landsat; Debris-Covered Glaciers; Glacial Lakes; Remote Sensing.

Highlights

- 1989–2017 Chandra Valley glacier change mapped from Landsat and DEM
- Total glacier area −15%; glacial lakes +51% (feature-resolved)
- Results inform water planning and GLOF risk screening

1 Introduction

Mountain glaciers in the Western Himalaya are retreating, reshaping water availability, sediment regimes, ecosystems, and hazards such as glacial lake outburst floods (GLOFs). Medium-resolution satellite archives now allow consistent, multi-decadal mapping, yet three gaps remain common: (i) debris-covered ice is hard to delineate automatically; (ii) many studies report only total glacier area, masking internal reorganization; and (iii) glacial lakes are often mapped separately, limiting coupled glacier–lake interpretation.

The Chandra Valley is an ideal setting to address these gaps: it hosts debris-rich valley glaciers, strong elevation gradients, and rapidly evolving proglacial zones that affect downstream communities and infrastructure. A compact, feature-resolved assessment across multiple time slices can reveal not only the magnitude of change but also *where* and *how* glacier landscapes are transforming.

We present a four-epoch (1989, 2001, 2009, 2017), feature-wise analysis using Landsat TM/OLI imagery and a supporting DEM. Beyond total glacier area, we quantify five elements that characterize glacier state and its forefield: accumulation area, ice-exposed ablation, debris-covered ablation, deglaciated valley, and glacial lakes. Changes are examined for three intervals (1989–2001, 2001–2009, 2009–2017) and the full period (1989–2017).

Our contributions are threefold: (1) a harmonized workflow that separates glacier components for targeted interpretation; (2) a coupled glacier–lake perspective that links lake growth with losses or redistribution among glacier features; and (3) interval diagnostics that test whether change is linear or period-specific. We report time-series trends, spatial change maps, and accuracy metrics, and we discuss implications for hydrology, GLOF screening, and ongoing monitoring in debris-rich Himalayan catchments.

2 Theoretical Background and Conceptual Framework

This section establishes the intellectual basis for analyzing glacier–landscape change in the Western Himalaya. It clarifies key concepts, synthesizes relevant theories and mapping frameworks, identifies gaps motivating this study, and proposes a concise conceptual model that links climatic drivers to feature-wise transitions and impacts (see Figure 1).

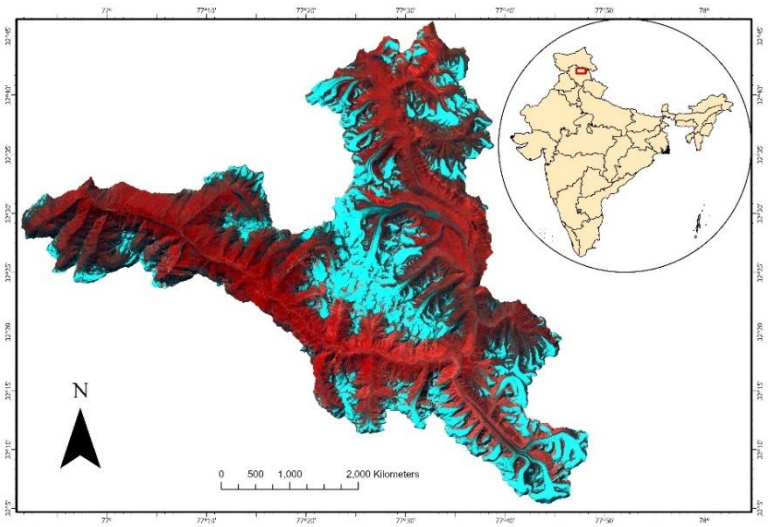

Figure 1. Chandra Valley study area

2.1 Defining Key Concepts

Glacier mass balance and zones. Glacier evolution reflects the balance between accumulation (snowfall, wind redistribution) and ablation (melt, sublimation). Spatially, glaciers comprise an accumulation area (AA) and an ablation area (AB) separated by the equilibrium-line altitude (ELA).

- Ablation sub-types. We distinguish ice-exposed ablation (IEA) from debris-covered ablation (DCA). Thick supraglacial debris can insulate ice (reducing melt), while thin/patchy debris can enhance melt; debris also fosters thermokarst and surface ponding.
- Deglaciated Valley (DV). Recently ice-free terrain recording retreat/downwasting; typically hosts moraines, outwash, and paraglacial slope adjustment.
- Glacial lakes (GL). Supraglacial/proglacial water bodies arising from downwasting and/or moraine/bedrock impoundment; sensitive indicators of retreat and potential GLOF sources.
- Operational definitions (this study). We map five elements—AA, IEA, DCA, DV, GL—at four epochs (1989, 2001, 2009, 2017) using harmonized Landsat imagery and DEM-supported rules, enabling feature-wise accounting rather than totals alone.
- *Real-world manifestation*. In debris-rich Himalayan tongues, clean-ice area often shrinks while DCA persists or grows; proglacial lakes expand where tongues thin and ponding stabilize behind moraines.

2.2 Existing Theories and Frameworks

- Cryospheric response. Warming and ELA rise drive AA contraction and AB expansion/reshaping; debris modulates melt (insulation vs enhancement), promoting tongue stagnation and thermokarst development.
- Paraglacial adjustment. Ice retreat triggers transient increases in sediment supply and landscape reworking within DV, influencing fluvial systems.
- Lake evolution and hazards. Coupled glacier–lake dynamics link downwasting to GL growth and GLOF susceptibility where dams are unconsolidated or ice-cored.
- Remote-sensing frameworks. Clean ice/snow are well captured by spectral indices; debris-covered ice requires hybrid approaches (spectral + terrain/object rules + visual QA). Multi-epoch change detection benefits from consistent seasonality/geometry and per-class accuracy assessment.
- Strengths/limitations. Spectral indices are robust for IEA/AA but conflate DCA with surrounding moraines; DEM/context rules improve DCA mapping but add analyst judgement; interval analyses clarify nonlinearity but require careful sensor harmonization.

2.3 Knowledge Gaps and Research Opportunities

- Aggregation bias: Many studies report total glacier area only, obscuring internal reorganization among AA, IEA, DCA, DV, and GL.
- Debris complexity: Automated DCA delineation remains uncertain; few works present feature-resolved accuracy alongside change magnitudes.
- Coupled dynamics: Glacier and lake changes are often analyzed separately, limiting process-consistent interpretation of hazard emergence.
- Temporal diagnostics: Interval-wise contrasts (e.g., 1989–2001 vs 2001–2009 vs 2009–2017) are underused, yet essential to detect nonlinearity and climate-phase effects.

This study addresses these gaps by delivering a harmonized, feature-wise multi-epoch account, coupling glacier features with lakes, quantifying interval changes, and reporting year-wise accuracy to bound interpretation.

2.4 Proposed Conceptual Model

Structure (driver–state–impact):

Drivers: regional temperature/precipitation variability; ELA rise; debris redistribution; ice dynamics.

State (features at each epoch): {AA, IEA, DCA, DV, GL}.

Transitions (expected):

AA ↓ with ELA rise;

IEA ↓ and DCA ↑ (debris concentration/stagnation phase), later stabilizing/declining as tongues detach;

AB → DV via retreat/downwasting;

AB/DCA → GL via thermokarst and moraine/bedrock impoundment.

Impacts: altered seasonal runoff/storage, enhanced paraglacial sediment flux, and GLOF risk where lakes expand behind unstable dams.

How the model guides the study.
(i) Quantify total and feature-wise trends across four epochs; (ii) diagnose interval changes and spatial hotspots; (iii) link lake growth to glacier-feature transitions; (iv) discuss hydrological and hazard implications within stated uncertainties.

Visual note: The model can be depicted as a schematic showing Drivers → (AA, IEA, DCA, DV, GL) with arrows for transitions (AA→AB; IEA→DCA; AB→DV; AB/DCA→GL) and an impact panel (runoff, sediment, GLOF).

3 Methodology

This study uses a quantitative, multi-epoch remote-sensing design to map glaciers and forefield changes in the Chandra Valley for 1989, 2001, 2009, and 2017. A hybrid workflow—combining spectral indices, terrain derivatives, and visual quality control—delineates five features: accumulation area (AA), ice-exposed ablation (IEA), debris-covered ablation (DCA), deglaciated valley (DV), and glacial lakes (GL). Changes are computed with post-classification comparison and reported as areas (km^2), interval deltas, and spatial hotspots. The overall process aligns with the methods flowchart (Fig. 2).

3.1 Research Design and Rationale

We adopt four discrete epochs and compare classified maps between epochs. This enables feature-wise accounting (beyond total glacier area) and interval diagnostics (1989–2001; 2001–2009; 2009–2017) to test for nonlinearity and to link glacier change with lake evolution.

3.2 Data Acquisition

We use cloud-free Landsat TM/ETM+/OLI scenes from late-ablation/early-autumn for the four years, plus an ALOS PALSAR (~12–30 m) DEM for elevation, slope, and curvature. All datasets are projected to WGS-84 / UTM Zone 43N. (Data sources and dates are summarized in Table 1.)

Table 1. Datasets and tools.

Dataset / Source	Platform / Sensor	Resolution	Year(s)	Path/Row	Key bands / info	Primary use
Landsat 5	TM	30 m (vis–SWIR); 120 m (TIR)	1989, 2001, 2009	147 / 37–38	VNIR, SWIR1–2, TIR	Glacier delineation & change detection
Landsat 8	OLI / TIRS	30 m (vis–SWIR); 15 m (Pan); 100 m (TIR)	2017	147 / 37–38	Coastal–SWIR2, Pan, TIRS1–2	Glacier delineation, pan-sharpened cartography
ALOS PALSAR DEM	—	12.5 m	2014	—	Elevation, slope, curvature	Terrain constraints & QA
Google Earth	High-res imagery	~0.5–2 m (varies)	1991, 2017	—	Visual reference	Manual QA / validation

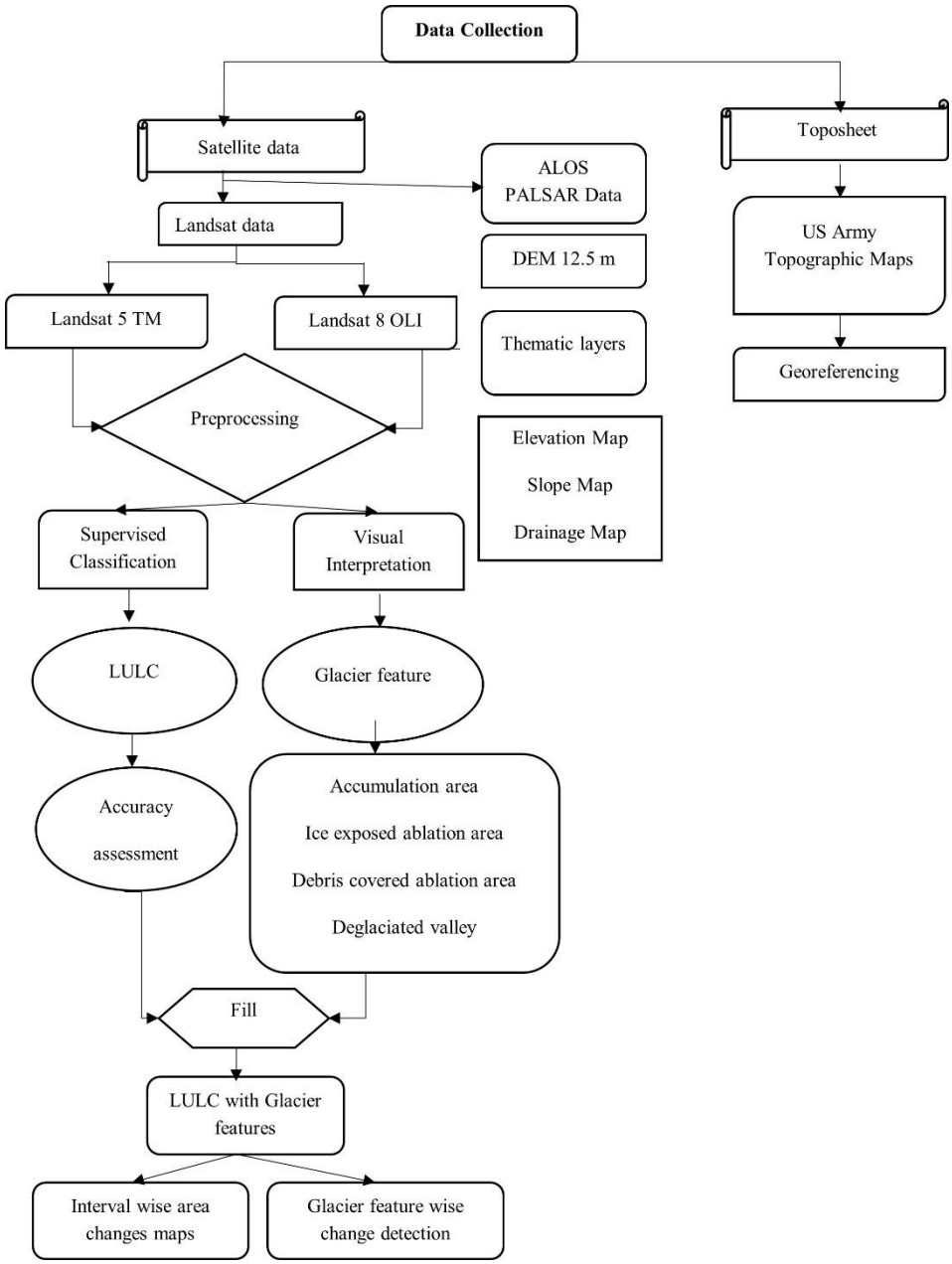

Figure 2. Workflow for multi-epoch mapping and change analysis.

3.3 Pre-processing

Radiometric handling uses surface-reflectance products where available; otherwise top-of-atmosphere reflectance is normalized across epochs. All rasters are co-registered to a common 30 m grid with RMSE < 0.5 pixel. Clouds and terrain shadows are removed using QA masks and manual edits. NDSI and DEM elevation bands suppress ephemeral snow while retaining persistent snow in AA.

3.4 Feature Mapping

Clean snow/ice (IEA/AA proxy) is extracted using NDSI + SWIR thresholds and brightness tests. Glacial lakes are mapped with NDWI/MNDWI tuned for topographic shadow, followed by manual QA in steep valleys. Debris-covered ablation is identified with a hybrid approach that combines low-albedo SWIR, slope (< ~25–30°), concavity, object/region cues, and hillshade checks to separate DCA from moraines/outwash. The AA–AB partition applies ELA-guided elevation bands with slope/aspect constraints. Deglaciated valley is defined as newly ice-free terrain contiguous with former glacier margins; perennial snowfields and stable bedrock are excluded with spectral-terrain stability tests.

3.5 Accuracy Assessment

We selected stratified random validation points per class and epoch, referencing high-resolution imagery with DEM context, and we report Overall Accuracy (OA), Kappa, and, where feasible, class-wise F1 (summary in Table 2).

Table 2. Accuracy assessment by epoch (validation N, OA, and Kappa).

Year	Validation samples (N)	Overall Accuracy (%)	Kappa
1989	113	74	0.66
2001	110	77	0.72
2009	119	83	0.79
2017	125	79	0.73

3.6 Change Detection and Metrics

Post-classification comparison yields transition matrices (e.g., AA→AB, IEA→DCA, AB→DV, AB/DCA→GL) for 1989–2001, 2001–2009, 2009–2017, and the net 1989–2017 change. Outputs include per-feature area by epoch, Δarea by interval, and spatial hotspot maps presented as a 2×2 composite.

3.7 Analysis, Cartography, and Reporting

Processing and metrics are implemented in QGIS/ArcGIS Pro and Python (rasterio, numpy, geopandas); figures use Matplotlib. Maps are exported at 300–600 dpi (TIFF/PNG) and as PDF/SVG with consistent color schemes and legends across years. We report Δarea alongside OA/Kappa and discuss uncertainties related to debris confusion, seasonal timing, sensor differences, and DEM artefacts. The study involves no human subjects; Landsat/DEM data are open, and derived layers are available upon request or via a repository.

4 Results – Key Findings

This section reports the main quantitative outputs in the order of the research questions and figures, without interpretation.

4.1 Total Glacier Area (1989–2017)

- Total glacier area decreased from 726.36 km^2 (1989) to 614.45 km^2 (2017), a net change of −111.91 km^2 (−15.41%).
- Year-wise totals used in Figure 3: 1989: 726.36, 2001: 621.70, 2009: 617.22, 2017: 614.45 km^2.

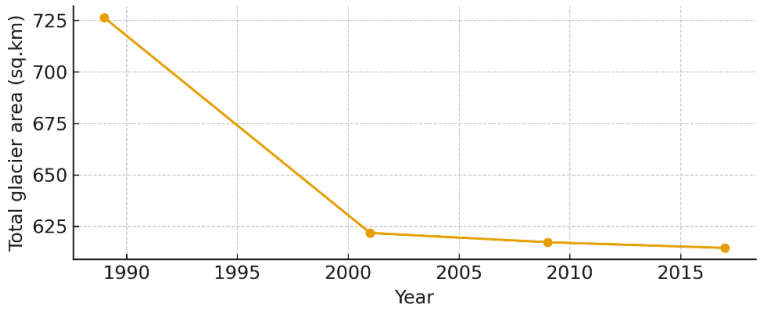

Figure 3. Total glacier area (km^2), 1989–2017.

4.2 Feature-Wise Areas by Epoch

Feature-wise areas (km^2) by epoch (2017–1989 net change; % relative to 1989; see Figure 4)

- Accumulation area (AA): 374.75 → 301.77 → 301.90 → 300.00 (−74.75, −19.95%)
- Ice-exposed ablation (IEA): 190.23 → 175.49 → 145.96 → 166.65 (−23.58, −12.39%)
- Debris-covered ablation (DCA): 161.39 → 144.44 → 169.36 → 147.80 (−13.59, −8.42%)
- Deglaciated valley (DV): 83.36 → 95.89 → 102.29 → 107.92 (+24.56, +29.46%)
- Glacial lakes (GL): 2.03 → 2.31 → 2.76 → 3.07 (+1.04, +51.23%)

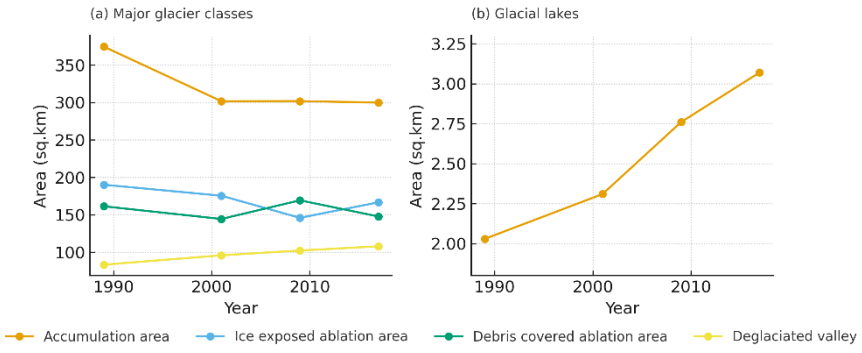

Figure 4. Feature-wise area trends (km^2), 1989–2017: (a) AA, IEA, DCA, DV; (b) glacial lakes

4.3 Interval Changes

(Δ = end − start of interval; km^2. Percentages are relative to the interval start value.)

1989 → 2001

- AA −72.98 (−19.5%); IEA −14.74 (−7.7%); DCA −16.95 (−10.5%); DV +12.53 (+15.0%); GL +0.28 (+13.8%)

2001 → 2009

- AA +0.13 (+0.0%); IEA −29.53 (−16.8%); DCA +24.92 (+17.3%); DV +6.40 (+6.7%); GL +0.45 (+19.5%)

2009 → 2017

- AA −1.90 (−0.6%); IEA +20.69 (+14.2%); DCA −21.56 (−12.7%); DV +5.63 (+5.5%); GL +0.31 (+11.2%)

4.4 Spatial Distributions

Valley-wide interval change. Figure 5 shows a 2×2 composite of glacier area-change maps for 1989–2001, 2001–2009, 2009–2017, and the net 1989–2017 change (shared legend).

Feature-specific changes. Figure 6 presents feature plates that overlay epochs for accumulation, ice-exposed ablation, debris-covered ablation, deglaciated valley, glacial lakes, and snout positions, revealing where each class reorganized through time.

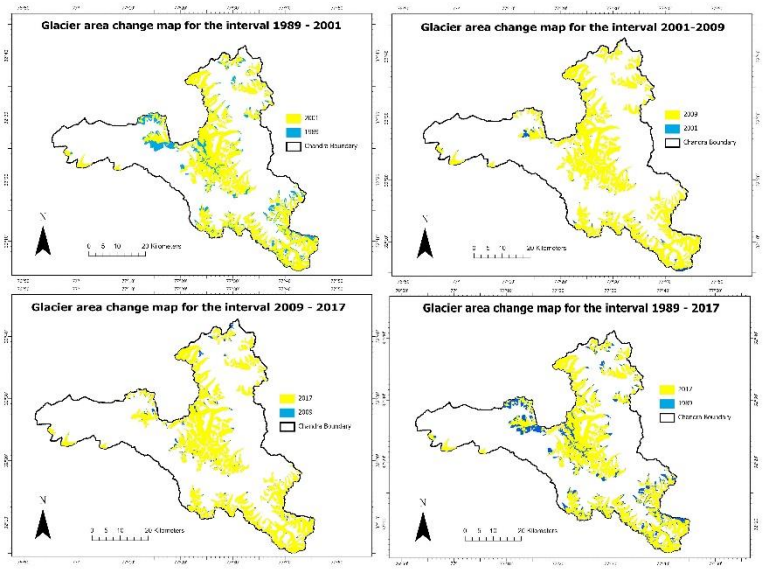

Figure 5. Area-change maps by interval—1989–2001, 2001–2009, 2009–2017—and net 1989–2017

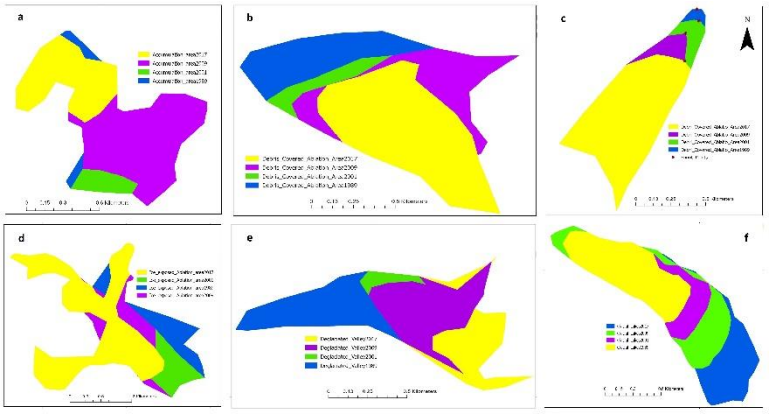

Figure 6. Feature-specific change across epochs: (a) accumulation, (b) debris-covered ablation, (c) snout position, (d) ice-exposed ablation, (e) deglaciated valley, (f) lakes

5 Discussion

Across four epochs (1989–2017) we observe a ~15% loss in total glacier area and strong internal reorganisation: AA contracted, IEA declined overall, DCA rose then receded, DV expanded, and GL increased by ~50%. Interval contrasts (1989–2001, 2001–2009, 2009–2017) indicate non-linear change, consistent with debris effects, downwasting, and basin-scale climate variability reported for the Western Himalaya. These shifts imply earlier/less reliable late-season runoff, and the growth of GL elevates GLOF screening priorities, especially where lakes expand adjacent to thinning tongues; DV expansion signals increased paraglacial sediment supply relevant to roads and hydropower corridors. Methodological uncertainties—debris–moraine spectral confusion, seasonal scene differences, cross-sensor radiometry, and DEM artefacts—are bounded by the reported accuracies but warrant caution for small differences. Future work should couple feature maps with ELA/snowline and climate series, expand lake-hazard analytics (dam type, freeboard, triggers), and apply higher-resolution/UAV mapping for debris and thermokarst detail. Overall, a feature-resolved, interval-aware lens clarifies where and how glacier surfaces and forefields are transforming, providing actionable evidence for water planning, infrastructure design, and risk management.

6 Conclusions

This study provides a feature-resolved, interval-aware assessment of glacier change in the Chandra Valley across four epochs (1989, 2001, 2009, 2017). Total glacier area declined by ~15% (−111.91 km^2), with marked internal reorganization: accumulation contracted, ice-exposed ablation decreased, debris-covered ablation rose then receded, deglaciated valley expanded, and glacial lakes grew by ~50%. Interval diagnostics (1989–2001, 2001–2009, 2009–2017) reveal non-linear trajectories, addressing gaps in totals-only assessments by coupling glacier features and lakes, reporting per-epoch accuracy, and mapping spatial hotspots.

Implications. The observed shifts indicate: (i) changes in seasonal runoff timing and reliability relevant to water supply and hydropower operations; (ii) elevated GLOF screening priorities where lakes expand near thinning tongues; and (iii) increased paraglacial sediment pulses affecting infrastructure siting and maintenance. The workflow (spectral–terrain hybrid mapping, post-classification comparison, feature accounting) is transferable to other debris-rich Himalayan catchments.

Limitations and future work. Uncertainties arise from debris–moraine spectral confusion, seasonal scene differences, cross-sensor radiometry, and DEM artefacts; these are bounded by year-wise accuracy metrics. Future research should integrate ELA/snowline and climate time series for attribution, expand lake-hazard analytics (dam type, freeboard, triggers), and exploit higher-resolution/UAV data for debris and thermokarst detail.

Overall, the study clarifies where and how glacier surfaces and forefields are transforming and provides actionable evidence for water-resource planning, infrastructure design, and risk management in the Western Himalaya.

Acknowledgements
The author thanks the home department for administrative and technical support and acknowledges open satellite data from USGS Landsat and the ALOS PALSAR DEM provider.

Funding
This research received no external funding.

Data Availability Statement
Landsat scenes and ALOS PALSAR DEM are openly available from their providers. Derived glacier masks, change layers, and scripts are available from the author upon reasonable request and will be deposited in a public repository upon acceptance.

Conflicts of Interest
The author declares no conflict of interest.

References

Bolch, T., Kulkarni, A., Kääb, A., Huggel, C., Paul, F., Cogley, J. G., … Stoffel, M. (2012). The state and fate of Himalayan glaciers. Science, 336(6079), 310–314.

Gardelle, J., Berthier, E., & Arnaud, Y. (2011). Slight mass gain of Karakoram glaciers in the early 21st century. Nature Geoscience, 5, 322–325.

Hall, D. K., Riggs, G. A., & Salomonson, V. V. (1995). Development of methods for mapping global snow cover using MODIS and NDSI. Photogrammetric Engineering & Remote Sensing, 61(3), 327–335.

Hugonnet, R., McNabb, R., Berthier, E., Menounos, B., Nuth, C., Girod, L., … Kääb, A. (2021). Accelerated global glacier mass loss in the early twenty-first century. Nature, 592, 726–731.

Kääb, A., Berthier, E., Nuth, C., Gardelle, J., & Arnaud, Y. (2012). Contrasting patterns of early twenty-first-century glacier mass change in the Himalayas. Nature, 488, 495–498.

McFeeters, S. K. (1996). The use of the Normalized Difference Water Index (NDWI) in the delineation of open water features. International Journal of Remote Sensing, 17(7), 1425–1432.

Paul, F., Bolch, T., Kääb, A., Nagler, T., Nuth, C., Scharrer, K., … Zemp, M. (2013). On the accuracy of glacier outlines derived from remote-sensing data. The Cryosphere, 7(6), 1565–1577.

Racoviteanu, A. E., Williams, M. W., & Barry, R. G. (2009). Optical remote sensing of glacier characteristics: A review with focus on the Himalaya. Remote Sensing of Environment, 113(5), 110–122.

Richardson, S. D., & Reynolds, J. M. (2000). An overview of glacial hazards in the Himalayas. Quaternary International, 65–66, 31–47.

Veh, G., Korup, O., & Walz, A. (2019). Hazard from Himalayan glacier lake outburst floods. Proceedings of the National Academy of Sciences, 116(7), 2544–2549.

Xu, H. (2006). Modification of normalised difference water index (NDWI) to enhance open water features: An MNDWI. International Journal of Remote Sensing, 27(14), 3025–3033.

Datasets / data providers

Japan Aerospace Exploration Agency (JAXA). (2014). ALOS PALSAR 12.5-m DEM [Data set]. Tokyo, Japan: JAXA. Retrieved from https://www.eorc.jaxa.jp/ALOS/en/ (Last Access: October 14, 2025).

U.S. Geological Survey (USGS). (2020). Landsat surface reflectance products (Collection 2) [Data set]. Reston, VA: USGS. Retrieved from https://www.usgs.gov/landsat (Last Access: October 14, 2025).

Software

Esri. (2021). ArcGIS Pro 2.7 [Computer software]. Redlands, CA: Esri. Retrieved from https://www.esri.com (Last Access: October 14, 2025).

Open-Source Geospatial Foundation. (2024). QGIS (Version 3.x) [Computer software]. Beaverton, OR: OSGeo. Retrieved from https://qgis.org (Last Access: October 14, 2025).

Python Software Foundation. (2022). Python (Version 3.10) [Programming language]. Wilmington, DE: Python Software Foundation. Retrieved from https://www.python.org (Last Access: October 14, 2025).

Disclaimer/Publisher's Note
The statements, opinions, and data contained in all publications are solely those of the individual author(s) and contributor(s) and do not reflect the views of the Architecture, Buildings, Construction and Cities (ABC2) Journal and/or its editor(s). ABC2 Journal and/or its editor(s) disclaim any responsibility for any injury to people or property resulting from any ideas, methods, instructions, or products referred to in the content.